Analysis of carriers dynamics and laser emission in 1.55 μm InAs/InP(113)B quantum dot lasers

Jacky Even*[a], Frédéric Grillot[a], Kiril Veselinov [a], Rozenn Piron [a], Charles Cornet [a], François Doré[a],
Laurent Pedesseau[a], Alain Le Corre[a], Slimane Loualiche[a], Patrice Miska[b], Xavier Marie[c],
Mariangella Gioannini[d], Ivo Montrosset[d]

[a]CNRS, INSA de Rennes, FOTON, Fonctions Optiques pour les Technologies de l'informatiON ,
CS70839, 35708 Rennes Cedex, France
[b]CNRS, Université de Nancy, UPV Metz, Institut Jean Lamour, Faculté des Sciences, Boulevard des
Aiguillettes, BP239, 54506 Vandoeuvre-lès-Nancy, France
[c]CNRS, Université de Toulouse, INSA, UPS, LPCNO, 135 Avenue de Rangueil, 31077 Toulouse
Cedex 4, France
[d]Dipartimento di Elettronica, Politecnico di Torino, Corso Duca degli Abruzzi, 24, Torino (Italy)

ABSTRACT

Thanks to optimized growth techniques, a high density of uniformly sized InAs quantum dots (QD) can be grown on InP(113)B substrates. Low threshold currents obtained at 1.54 μm for broad area lasers are promising for the future. This paper is a review of the recent progress toward the understanding of electronic properties, carrier dynamics and device modelling in this system, taking into account materials and nanostructures properties. A first complete analysis of the carrier dynamics is done by combining time-resolved photoluminescence experiments and a dynamic three-level model, for the QD ground state (GS), the QD excited state (ES) and the wetting layer/barrier (WL). Auger coefficients for the intradot assisted relaxation are determined. GS saturation is also introduced. The observed double laser emission for a particular cavity length is explained by adding photon populations in the cavity with ES and GS resonant energies. Direct carrier injection from the WL to the GS related to the weak carrier confinement in the QD is evidenced. In a final step, this model is extended to QD GS and ES inhomogeneous broadening by adding multipopulation rate equations (MPREM). The model is now able to reproduce the spectral behavior in InAs-InP QD lasers. The almost continuous transition from the GS to the ES as a function of cavity length is then attributed to the large QD GS inhomogeneous broadening comparable to the GS-ES lasing energy difference. Gain compression and Auger effects on the GS transition are also be discussed.

Keywords: laser, quantum dot, semiconductor, Auger effect

1. INTRODUCTION

Recently, the development of self-organized InAs QDs on misoriented InP(113)B substrates has been proposed to get QDs with both quantum sizes and a high surface density[1]. The growth of these QDs is particular, yielding, via the control of the maximum QD height of the sample, the control of their wavelength emission. These structures emit then at 1.55 μm at room temperature. The optical properties of a single QD layer have been analyzed, and lasing structures were obtained with such nanostructures[2, 3]. Nevertheless, a dynamic analysis, is necessary to give precise information for the description of the properties of a 1.55 μm InAs/InP laser. In this paper, a theoretical model starting from the basic physical properties of the QDs, is used to investigate the lasing spectrum properties of 1.55μm InAs/InP (113)B QD lasers. The final numerical model used is based on a multi-population rate equation model (MPREM). It takes into account the effect of the competition between the inhomogeneous broadening (due to the QD size dispersion) and the homogenous broadening as well as a nonlinear gain variation associated to a multimode laser emission. The double laser emission and the temperature dependence of lasing spectra of self-assembled InAs/InP quantum dot lasers are studied theoretically. New refinements of the model are proposed.

2. DYNAMIC THREE-LEVELS MODEL FOR TIME-RESOLVED PHOTOLUMINESCENCE EXPERIMENTS

2.1 Electronic properties of InAs/InP(113)B QDs

Quantum sizes, high surface densities and ultralow threshold current in broad area lasers have been obtained for self-organized InAs QDs grown on misoriented InP(113)B substrates. The QDs are obtained by the spontaneous Stranski-Krastanow growth mode after the deposition of 2.1 InAs monolayers (ML) at 480°C on InP(311)B substrate with a gas source molecular beam epitaxy system. The double-cap (DC) growth method is then used to control the QD maximum height. Fundamental studies of the electronic properties of InAs/InP (113)B were performed with state of the art 8x8 k.p modeling of QD monoelectronic states including strain[4]. Multiexcitonic properties were simulated by adding many-body effects for few particles states like excitons, biexcitons or charged trions, in good agreement with available experimental results. The GS transition appears mainly associated to a pair of S-like monoelectronic states. The exciton binding energy is equal to about 15 meV with a weak dependence on QD geometry. The biexciton binding energy is equal to about 1meV for QD emitting at 1.55μm. It can be neglected by comparison to the inhomogeneous (equal to at least 45meV) or the homogeneous line broadenings introduced in figure 1. The photon emissions from the GS exciton and GS biexciton states can only be separated by using single QD spectroscopy at low temperature[5]. A single GS energy level with double occupancy is considered in the dynamical model. Figure 1 shows also an energy splitting between the two ES which are associated to P-like monoelectronic states. This energy splitting (10 meV) is again smaller than the experimental broadening. It is neglected in the dynamical rate equation model (REM) and a double degeneracy is considered for the ES.
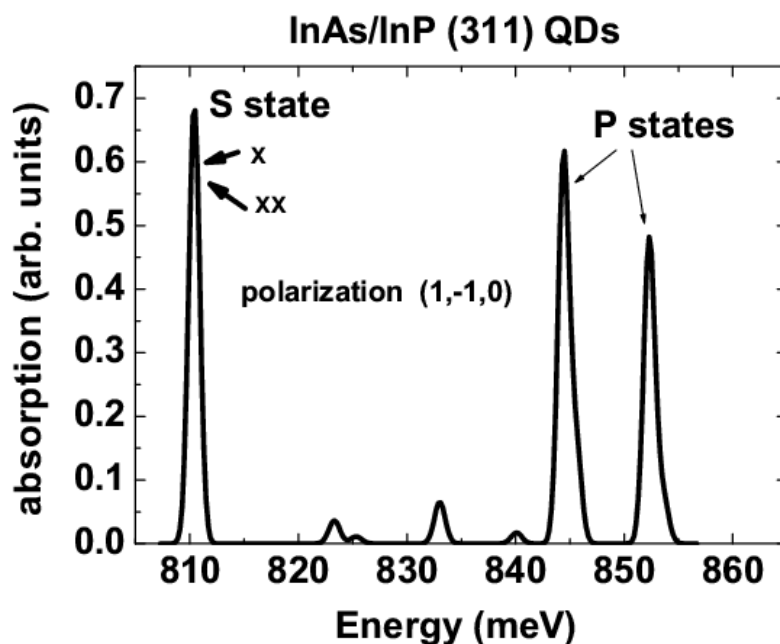

Figure 1. Calculated optical absorption spectrum for a single InAs/InP QD on a single InP(113)B substrate. The GS transition is mainly associated to S-like monoelectronic states while the doubly degenerated ES corresponds to P-like monoelectronic states. X and XX symbols indicate that excitonic and biexcitonic GS emit roughly at the same energy.

The effect of substrate misorientation, (113)B versus (001), is small. Weak S-P transitions are indeed predicted between S states and P states transitions (figure 1). These transitions which are forbidden by symmetry on (001) substrates, are neglected in the dynamical REM.

2.2 Optical properties of InAs/InP(113)B QDs

InAs/InP(113)B QD samples were characterized by time-resolved photoluminescence spectroscopy (tr-PL) at low temperature[6,7]. The experiments were performed using a 790 nm Ti-Sapphire laser (excitation in the InP barrier) producing 1.2 ps-long light pulses with a repetition rate of about 82 MHz. The tr-PL were then recorded by using either a streak camera or up-converting the luminescence signal in a nonlinear crystal. The spectra were fitted with three peaks at energy positions corresponding to the excitonic states: the GS and ES transitions in the QD, and the wetting layer excitonic ground state (WL). In addition a WL excited state can be observed if the excitation density is strong. At short times, the emission of the WL state is the most important one. GS emission is however also observed, and attributed to direct carrier injection channels from the barrier. For longer times, carrier populations in high energy states diminish either by light emission or by relaxation to ES or GS. Figure 2 represents the kinetics of light emission from the GS and ES at weak (50 W.cm^{-2}) excitation density. The spontaneous radiative decay time constant for the GS emission is equal to about 1200ps. It is smaller for the ES emission.
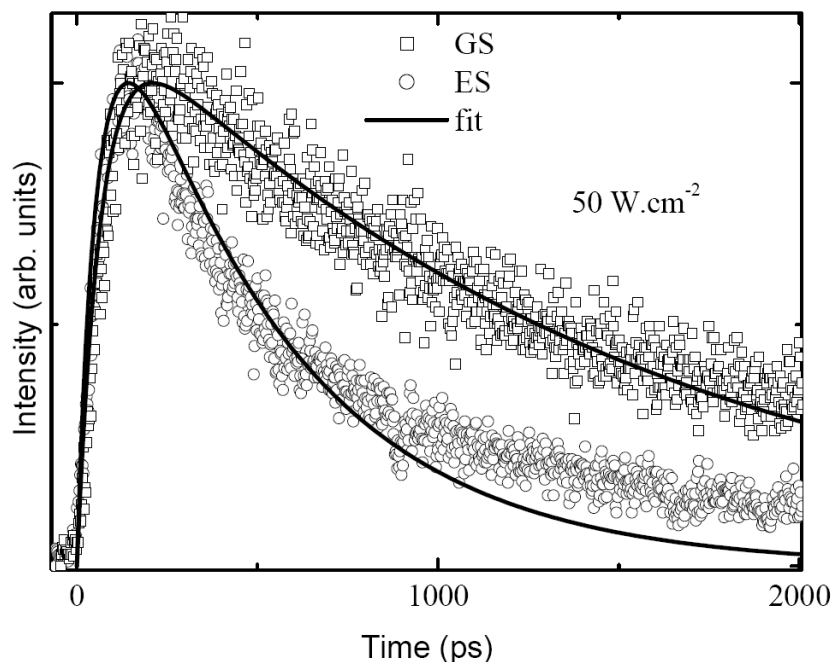

Figure 2. Kinetics of light emission from the GS and ES at weak (50W.cm-2) excitation density measured by time-resolved photoluminescence spectroscopy (tr-PL) at low temperature (10K).

The lifetimes of the three energy levels (GS, ES and WL) can be measured simultaneously in a streak camera experiment. A REM with a cascade relaxation of excitons[8] between the three considered levels is not able to describe correctly the experimental kinetics. A direct relaxation of carriers (τ_{GS}^{WL}) from the WL to the GS was added to the REM (figure 3). When the temperature or excitation increases, an efficient emptying of the WL toward the GS can be observed. The WL decay time becomes shorter. This evolution happens together with a slight increase of the GS PL intensity, a slight decrease of the WL PL intensity, and the GS emission spectral width enlargement. This evolution with temperature can be interpreted, as a carrier relaxation assisted by phonon emission. The ES decay time becomes also shorter. This evolution is typical of an Auger relaxation process toward GS. The Auger and phonon relaxation processes have been analyzed by measuring the tr-PL GS and ES rise times as a function of both excitation density and temperature.
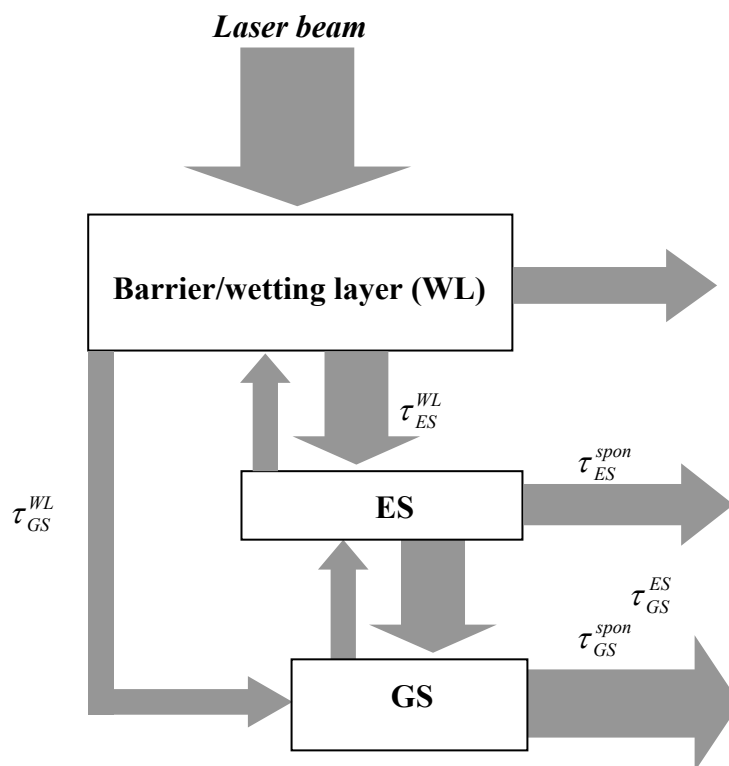
Figure 3. Schematic representation of the carrier dynamics with direct relaxation channel from the WL to the GS.

Under high excitation density, the rise times of both levels are independent of temperature. The Auger relaxation process is then dominant (figure 4).
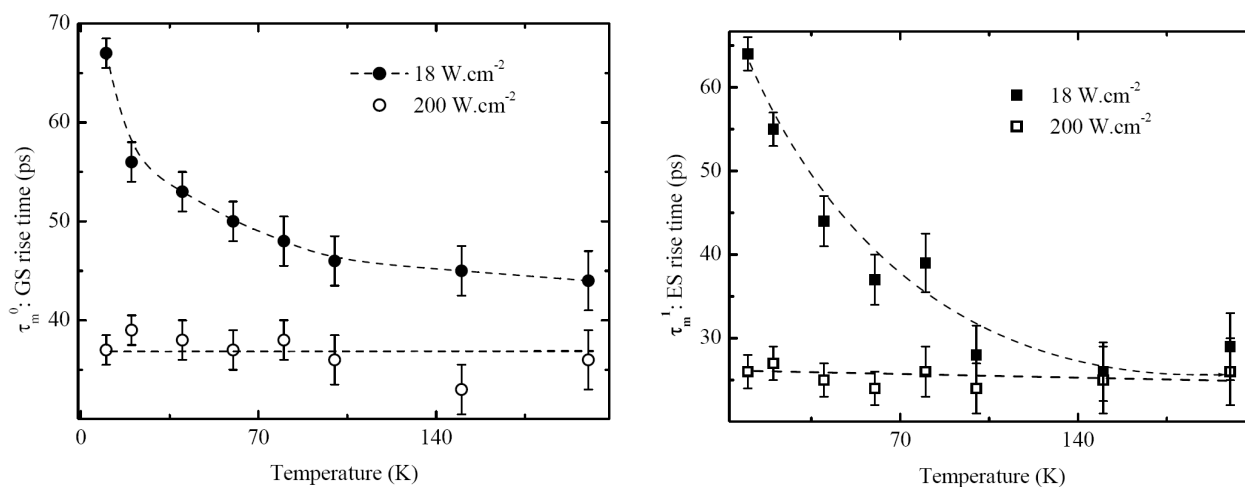
Figure 4. GS (left) and ES (right) rise times as a function of temperature for weak (18 W.cm^{-2}) and strong (200 W.cm^{-2}) excitation densities.

On the contrary, under weak excitation density, the rise times decrease with temperature. This reveals a strong influence of the phonon relaxation which is the dominating process in this regime.

2.3 Three levels rate equation model

The three level REM similar to the one used in ref. [9], also include also include eh-pairs escape times (τ_{WL}^{GS}, τ_{WL}^{ES}):

$$\frac{dN_{WL}}{dt} = \frac{I}{e} + \frac{N_{ES}}{\tau_{WL}^{ES}} - \frac{N_{WL}}{\tau_{ES}^{WL}} f_{ES} - \frac{N_{WL}}{\tau_{GS}^{WL}} f_{GS} - \frac{N_{WL}}{\tau_{WL}^{spon}}$$

$$\frac{dN_{ES}}{dt} = \frac{N_{WL}}{\tau_{ES}^{WL}} f_{ES} + \frac{N_{GS}}{\tau_{ES}^{GS}} f_{ES} - \frac{N_{ES}}{\tau_{WL}^{ES}} - \frac{N_{ES}}{\tau_{GS}^{ES}} f_{GS} - \frac{N_{ES}}{\tau_{ES}^{spon}}$$

$$\frac{dN_{GS}}{dt} = \frac{N_{WL}}{\tau_{GS}^{WL}} f_{GS} + \frac{N_{ES}}{\tau_{GS}^{ES}} f_{GS} - \frac{N_{GS}}{\tau_{ES}^{GS}} f_{ES} - \frac{N_{GS}}{\tau_{GS}^{spon}}$$

eh-pairs escape times are derived from a detailed balance analysis where a quasi-thermal equilibrium is assumed for the system and Fermi distributions are used for the carrier populations. $N_{ES,GS, WL}$ are the ES, GS and WL carrier numbers. $f_{ES,GS}$ are the ES and GS occupation factors which depend on carrier numbers, QD density and ES double degeneracy. These occupation factors must be included to simulate the saturation effect occurring in the GS at high excitation densities. The WL is considered as a charge carrier storage with infinite capacity. Auger processes involving a WL carrier captured directly into the GS or the ES by transferring its energy to a second WL carrier, are calculated through phenomenological relations:

$$\tau_{GS}^{WL} = \frac{1}{A_W + C_W N_{WL}} \quad \text{and} \quad \tau_{ES}^{WL} = \frac{1}{A_W + C_W N_{WL}}$$

A similar relation is used for the Auger assisted relaxation from the ES to the GS: $\tau_{GS}^{ES} = \frac{1}{A_E + C_E N_{WL}}$

A_W (A_E), C_W (C_E) are the coefficients for phonon and Auger-assisted capture (relaxation) respectively. With these phenomenogical relations, it was possible to reproduce the experimental results obtained by tr-PL.

3. ANALYSIS OF LASER EMISSION

3.1 Two-state laser emission in optical pumped InAs/InP(113)B QD laser

Recent experimental studies conducted on QD lasers have shown that a second laser peak may appear in the laser spectrum as increasing the injection power. This two-state laser emission is indeed a common property which has already been observed first for the InGaAs/GaAs systems[10]. In the case of InAs/InP(113)B QD laser, the same effect was observed for a diode laser which was composed of an active region with six InAs QD stacked layers[11]. The cavity length was 2.45 mm with cleaved uncoated facets while the width of the strip is 120 µm. The optical pumped structure was operating at room temperature under $1.06\mu m$ pulsed excitation. Only spontaneous emission form the GS is measured at low optical excitation. With increasing the optical excitation, laser emission occurs at $1.51\mu m$ (GS). With increasing pumping power density the emission intensity increases. Then a second stimulated emission appears at $1.43\mu m$ (ES). Experiments also have shown that the GS emission keeps growing (even if the ES starts lasing) without a significant broadening of the GS line. This effect has been attributed to the direct relaxation channel from the WL to the GS in order to describe properly the behaviour of QD lasers grown on InP[12]. The impact of the two-state laser emission on the light current characteristic can be properly explained by extending the three level REM to include the ES and GS photon numbers $S_{ES,GS}$:

$$\frac{dN_{WL}}{dt} = \frac{I}{e} + \frac{N_{ES}}{\tau_{WL}^{ES}} - \frac{N_{WL}}{\tau_{ES}^{WL}} f_{ES} - \frac{N_{WL}}{\tau_{GS}^{WL}} f_{GS} - \frac{N_{WL}}{\tau_{WL}^{spon}}$$

$$\frac{dN_{ES}}{dt} = \frac{N_{WL}}{\tau_{ES}^{WL}} f_{ES} + \frac{N_{GS}}{\tau_{ES}^{GS}} f_{ES} - \frac{N_{ES}}{\tau_{WL}^{ES}} - \frac{N_{ES}}{\tau_{GS}^{ES}} f_{GS} - \frac{N_{ES}}{\tau_{ES}^{spon}} - N_B \Gamma v_g a_{ES} \left(\frac{N_{ES}}{2N_B} - 1 \right) \frac{S_{ES}}{(1 + \varepsilon_{ES} S_{ES})}$$

$$\frac{dN_{GS}}{dt} = \frac{N_{WL}}{\tau_{GS}^{WL}} f_{GS} + \frac{N_{ES}}{\tau_{GS}^{ES}} f_{GS} - \frac{N_{GS}}{\tau_{ES}^{GS}} f_{ES} - \frac{N_{GS}}{\tau_{GS}^{spon}} - N_B \Gamma v_g a_{GS} \left(\frac{N_{GS}}{N_B} - 1 \right) \frac{S_{GS}}{(1 + \varepsilon_{GS} S_{GS})}$$

$$\frac{dS_{ES}}{dt} = N_B \Gamma v_g a_{ES} \left(\frac{N_{ES}}{2N_B} - 1 \right) \frac{S_{ES}}{(1 + \varepsilon_{ES} S_{ES})} - \frac{S_{ES}}{\tau_p} + \beta_{sp} \frac{N_{ES}}{\tau_{ES}^{spon}}$$

$$\frac{dS_{GS}}{dt} = N_B \Gamma v_g a_{GS} \left(\frac{N_{GS}}{N_B} - 1 \right) \frac{S_{GS}}{(1 + \varepsilon_{GS} S_{GS})} - \frac{S_{GS}}{\tau_p} + \beta_{sp} \frac{N_{GS}}{\tau_{GS}^{spon}}$$

The ES and GS linear gain coefficients $a_{ES,GS}$ were deduced from a direct measurement of InAs/InP QDs absorbance with a Fourier transform infrared spectrometer[13]. The sample was a 12-stack InAs quantum dots grown by molecular beam epitaxy on (311)B InP oriented substrate. The absorption coefficient was estimated at 4400 cm^{-1} for 3 nm height QDs and a 5x10^{10} cm^{-2} surface QD density. The absorption of the QD structures was found to be similar to quantum well structures when the number of atoms considered absorbing is equivalent. Gain compression coefficients $\varepsilon_{ES,GS}$ were included in the REM but set to zero for the first simulations.

3.2 Effects of the temperature on the lasing characteristic

Lasing and electroluminescence spectra were studied as a function of temperature under pulsed electrical injection for a conventional edge emitting laser with a 100 μm wide ridge structure formed by wet chemical etching. A drastic narrowing of the electroluminescence spectra was observed with increasing temperature. Thus, at low temperature, a very broad-band multimode lasing spectra up to 26 meV width (50 nm) at high injection current was observed. The laser emission progressively narrows with rising temperature, leading to spectra with a width of 2.8 meV (6 nm) at 253K. The observed temperature dependence of lasing spectra can be explained qualitatively by taking into account the homogeneous broadening of the optical gain of a single dot. At low temperature, when the homogeneous broadening is negligible, dots with different energies have a relatively narrow individual optical gain (narrow single dot linewidth with a FWHM below 2nm[14]) and since they are spatially isolated from each other, there is no correlation between the individual emissions. Then, all dots that have an optical gain above the lasing threshold start lasing independently, leading to broad-band lasing emission. On the other hand, when homogeneous broadening is comparable to inhomogeneous broadening, lasing mode photons are emitted not only from energetically resonant dots but also from other non-resonant dots within the range of the homogeneous broadening. This leads to a collective lasing emission with narrow line of a dot ensemble which explains the emission spectra observed close to room temperature.

3.3 Multipopulation rate equation model

The experimental results on the effects of temperature were explained by extending the REM to include multipopulation of QD and photons[15, 16]:

$$\frac{dN_{WL}}{dt} = \frac{I}{e} + \sum_n \frac{N_{ESn}}{\tau_{WLn}^{ES}} + \sum_n \frac{N_{GSn}}{\tau_{WLn}^{GS}} - \frac{N_{WL}}{\tau_{ES}^{WL}} - \frac{N_{WL}}{\tau_{WL}^{spon}} - \frac{N_{WL}}{\tau_{GS}^{WL}}$$

$$\frac{dN_{ESn}}{dt} = \frac{N_{WL}}{\tau_{ESn}^{WL}} + \frac{N_{GSn}(1-P_{ESn})}{\tau_{ESn}^{GS}} - \frac{N_{ESn}}{\tau_{WLn}^{ES}} - \frac{N_{ESn}}{\tau_{GSn}^{ES}} - \frac{N_{ES}}{\tau_{ES}^{spon}} - \frac{c\Gamma}{n_r}\sum_m g_{mnES} S_m$$

$$\frac{dN_{GSn}}{dt} = \frac{N_{ESn}}{\tau_{GSn}^{ES}} + \frac{N_{WL}}{\tau_{GSn}^{WL}} - \frac{N_{GSn}(1-P_{ESn})}{\tau_{ESn}^{GS}} - \frac{N_{GSn}}{\tau_{WLn}^{GS}} - \frac{N_{GS}}{\tau_{GS}^{spon}} - \frac{c\Gamma}{n_r}\sum_m g_{mnGS} S_m$$

$$\frac{dS_m}{dt} = \frac{c\Gamma}{n_r}\sum_n (g_{mnES} + g_{mnGS})S_m - \frac{S_m}{\tau_p} + \beta\sum_m \left(B_{ES}(E_m - E_{ESn})\frac{N_{ES}}{\tau_{ES}^{spon}} + B_{GS}(E_m - E_{GSn})\frac{N_{GS}}{\tau_{GS}^{spon}} \right)\Delta E_m$$

where $m = 0,1,...,M-1$ and $n = 0,1,...,N-1$ describe respectively the longitudinal modes of the cavity and the QD sub-group in the active region.

The material gain is described by the set of equations:

$$g_{mnES} = \mu_{ES} \frac{\pi e^2 \hbar}{c n_r \varepsilon_0 m_0^2} \frac{N_d}{H} \frac{|P_{ES}^\sigma|^2}{E_{ESn}} (2P_{ESn} - 1) G_{nES} B_{ES}(E_m - E_{ESn})$$

$$g_{mnGS} = \mu_{GS} \frac{\pi e^2 \hbar}{c n_r \varepsilon_0 m_0^2} \frac{N_d}{H} \frac{|P_{GS}^\sigma|^2}{E_{GSn}} (2P_{GSn} - 1) G_{nGS} B_{GS}(E_m - E_{GSn})$$

where H is the average height of the QD and $|P_{ES,GS}^\sigma|^2$ is the density matrix momentum. The various QD populations are coupled by the homogenous broadening of the stimulated emission process assumed to be Lorentzian:

$$B_{ES,GS}(E_m - E_{ESn,GSn}) = \frac{\Gamma_{hom}/2\pi}{(E_m - E_{ESn,GSn})^2 + (\Gamma_{hom}/2)^2}$$

with Γ_{hom} being the FWHM of the homogeneous broadening and E_m being the mode energy. Using the MPREM, Figure 5 shows in the case of the two-state lasing that the optical spectrum depends on the value of Γ_{hom}.

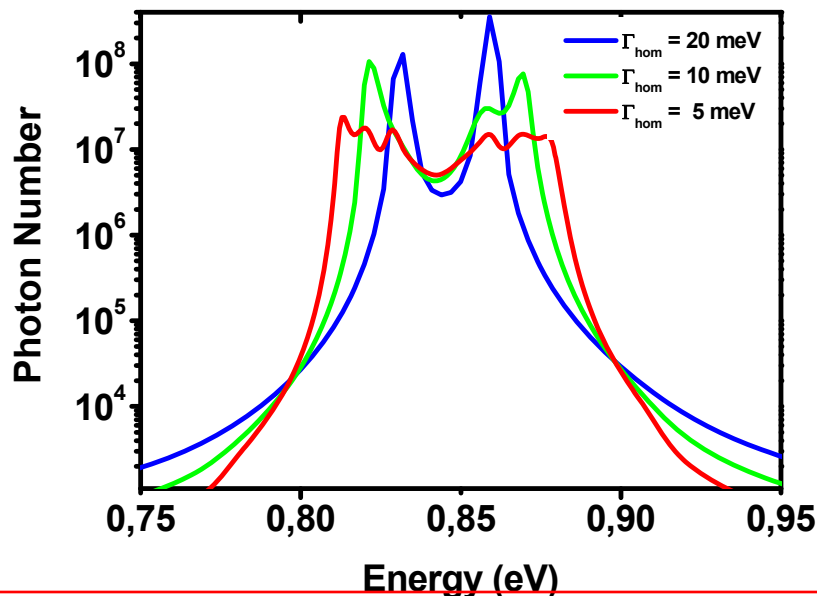SPIE USE: _____ DB Check, _____ Prod Check, Notes:

Figure 5. Calculated lasing spectra showing two-state laser emission at fixed current injection for different values of the homogeneous broadening width

3.4 Effects of the cavity length on the lasing characteristic

In the case of InAs–InP(113)B QD lasers, a continuous transition from the GS toward the ES is observed when decreasing the cavity length. The GS always contributes to lasing emission but its contribution decreases as long as the lasing wavelength moves from longer to shorter wavelength. This result is strengthened by the fact that both calculations with the MPREM and experimental results are in a relative good agreement. This continuous transition has never been observed in the InAs–GaAs system since lasing wavelength switches drastically on the ES as reported in[10]. This is because the spreading in QD size distribution in InAs–GaAs system is not as important as in the InAs–InP system. The inhomogeneous broadening is about 40–50 meV instead of 70 meV at room temperature on InP substrates. Furthermore, a better carrier confinement into the QD is usually obtained on GaAs and this determines a larger energy separation between the GS and the ES (meV) compare to the InAs–InP system (meV). Consequently, in the InAs–InP system, a spectral overlap between the GS and the ES gain occurs. As a consequence of the significant gain overlap, a continuous variation of the gain peak from the GS to the ES energy when current density is increased.

4. FURTHER IMPROVEMENT OF THE MODEL

4.1 Biexciton radiative lifetime

Using tr-PL experiment, the spontaneous radiative decay time constant for the GS emission was found to be equal to about 1200ps. Using time-resolved pump probe experiment under high resonant excitation[17], we were also able to measure carrier radiative lifetime and differential transmission. The exciton and biexciton lifetimes were measured to be about 1720ps and 530ps. It is possible to use this result and refine the model by introducing a dependence of τ_{GS}^{spon} on the GS occupancy factor f_{GS}.

4.2 Interband Auger effect

It is known from experimental results, particularly in InAs/InP QDs devices[18], that non-radiative Auger processes on the main interband optical transition can be significant. Strangely, these last phenomena are not much described from the theoretical point of view. First studies on QDs even claim that these processes are either forbidden or at least negligible due to weak overlap integrals between mostly s-type wave function associated to conduction band and mostly p-type wave function for the valence band . For that reason, the interband Auger rates were not considered in the study of GaAs quantum dots[19]. However, interband Auger recombination processes have been recognized for a long time as important in bulk materials or quantum wells (QW) with small band gap energies. To simplify the simulation of InAs/InP QDs electronic properties and Auger effects, we used our model recently proposed[20] where QD geometries corresponding to the $C_{\infty v}$ symmetry are considered and complex inhomogeneous strain distribution are taken into account using only cylindrical coordinates (r,z).

We simulate in the following Auger mechanisms involving the non-radiative transitions of an electron between two states in the QD associated to a transition of another electron (or hole) in the continuum. Figure 6a represents the variation of the radiative lifetime as a function of the interband transition energy in the case of a truncated conic QD where the truncation height varies (TH) (radius R=17.5nm and full-cone height H=8.8nm). The overlap term between electron and hole ground states plays a crucial role in the Auger process and is different from the ones of the radiative transitions. In the limit of a complete CB-VB decoupling (in the case of a large gap), the Auger processes associated to the interband transitions vanish and the variations of the overlap term for intraband transitions in the CB can be predicted from a simple one band model. By analogy to interband Auger processes in bulk materials, the non radiative interband process in the QDs is associated to a transition in the bulk CB (CHCC), or from the SO band to HH band (CHSH) or from the LH band to HH band (CHLH). The CHSH is the most important one because the spin-orbit splitting energy of the InGaAsP alloy is smaller but on the order of the gap energy. Curves (b) and (c) on figure 6 represent the variations of

τ_{Aug} as a function of the energy gap for the same truncated cone QD for a hole (CHSH) or an electron (CHCC) concentration equal to 10^{18}cm^{-3}. This variation is mainly associated to the decoupling of the CB and VB QD states when the energy gap opens.
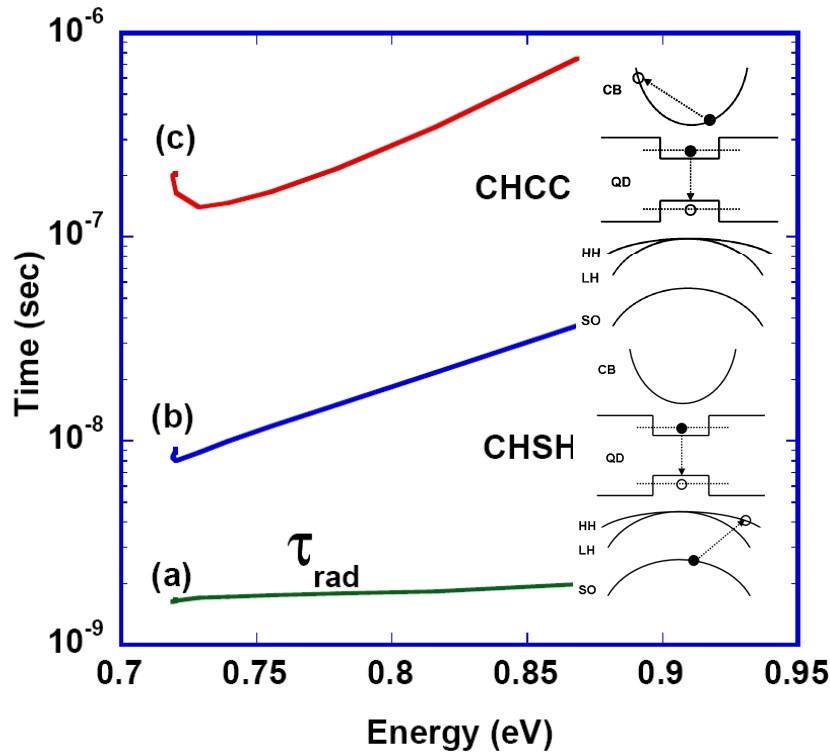

Figure 6. Curve (a) represents the variation of radiative lifetime as a function of the energy gap. Variations of the Auger lifetimes are given as a function of the energy gap for the same truncated cone QD either for a hole (CHSH, (b)) or an electron (CHCC, (c)) concentration equal to 10^{18}cm^{-3}. The insert shows schematic views of the CHCC and CHSH processes.

We propose to include the CHSH Auger effect by replacing $1/\tau_{GS}^{spon}$ by $1/\tau_{GS}^{spon} + C_{CHSH}N_{WL}$ where C_{CHSH} is a microscopic CHSH Auger coefficient that could be extracted from such a simulation. We may add that radiative lifetime τ_{GS}^{spon} and intraband Auger effects are well reproduced by this model.

4.3 Gain compression

The effects of the nonlinear gain in a QD laser have shown that gain compression is systematically strengthened in such devices because of the gain saturation with carrier density[21]. In this section, the effects of the gain compression on the laser's light current characteristic (LCC) is studied. To account for the saturation of the optical gain generated by the semiconductor media with the photon density in the cavity, the compression terms $S_{ES,GS}/(1+\varepsilon_{ES,GS}S_{ES,GS})$ are included in the set of rate equations (section 3.1). Coefficients $\varepsilon_{ES,GS}$ are related to gain compression factors for the ground state (GS) and for the excited state (ES) respectively. The steady-state solution is obtained by a numerical calculation of the rate equations for a linear increase of the injection current density. Fig. 7(a) shows the calculated LCC without gain compression ($\varepsilon_{ES,GS} = 0$) and assuming the same laser parameters as those in section 3.1. Simulation demonstrates the occurrence of two thresholds corresponding to the two laser emissions. When the ES stimulated emission pops-up at 1000 A/cm^2, only a slight decrease of the GS slope efficiency is predicted. At the same time, the global slope efficiency increases. Thus, the inclusion of a direct relaxation channel points out that the double laser emission here results from an efficient carrier relaxation into the GS due to the pronounced Auger effect for larger injection rates. These results differ from the InAs/GaAs system on which once the second lasing of the ES appears, the emission of the GS saturates completely.
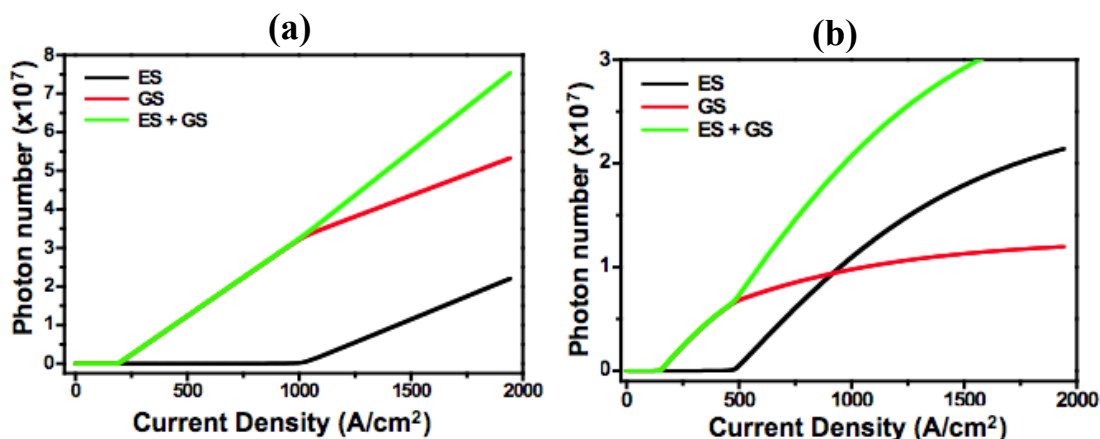
(a)   **(b)**

Figure 7. Calculated light-current characteristics of an 1.55µm InAs/InP(311)B QD laser (a) without gain compression (b) including gain compression

Fig. 7(b) shows the calculated LCC with non-zero gain compression factors ($\varepsilon_{ES,GS} \neq 0$). This simulation holds under the assumption that $\varepsilon_{GS}=\varepsilon_{ES}$. Including non-linearities in the rate equations lead to a significant deviation from fig. 7(a). Although the GS's threshold current does not change (~240 A/cm^2), simulations emphasize that the gain saturation in the GS through gain compression alters the shape of the LCC. Thus, the GS photon number which gets almost clamped at the highest injected current (2000 A/cm^2) is also decreased by a factor of 5 as compared to the case without compression. This saturation is associated to a reduction of the ES's threshold by a factor of 2 from 1000 A/cm^2 down to 500A/cm^2. Although the ES's LCC also saturates at larger pump current densities (not shown here), the photon number in the ES remains within the same order of magnitude as compared to fig. 7(a). Despite the global slope efficiency is still enhanced compression effects reduce the overall photon number and make the device moving faster on the ES. Next step to be investigated is to consider different values of factors $\varepsilon_{ES,GS}$ as well as to investigate compression effects on QD laser's turn-on dynamics which is relevant point for the realization and optimization of QD devices for optical communications.

5. CONCLUSION

In this paper, a MPREM is used to investigate the dynamics and lasing spectrum properties of InAs/InP (113)B quantum dot (QD) structures emitting at 1.55µm. The numerical model takes into account various basic physical properties of InAs/InP QDs. The saturation of the GS, the relaxational Auger effect and the two state lasing are correctly described. The effect of the competition between the inhomogeneous broadening and the homogenous broadening as well as a nonlinear gain variation associated to a multimode laser emission have been introduced. It has been shown that dots with different energies start lasing independently at low temperature due to their spatial localization while at room temperature the dot ensemble contributes to a narrow line lasing collectively via the homogeneous broadening of optical gain. Contrary to the case of InAs/GaAs QDs, the spectral overlap between the GS and the ES in InAs/InP QDs induces a continuous shift of the gain peak when the current density is increased. New developments of the model include Auger effect on the GS transition and gain compression. The numerical investigation based on the MPREM is important for the future optimization of InAs QDs lasers at 1.55µm on InP substrate.

*jacky.even@insa-rennes.fr; phone +33 223238295; fax +33 223238618; http://foton.insa-rennes.fr/efoton-insa.html

SPIE USE: _____ DB Check, _____ Prod Check, Notes:

REFERENCES

[1] Caroff, P., Paranthoën, C., Platz, C.,Dehaese, O., Folliot, H., Bertru, N., Labbé, C., Piron, R., Homeyer, E., LeCorre, A. and Loualiche, S., Appl. Phys. Lett., 87, 243107 (2005).

[2] Homeyer, E., Piron, R., Grillot, F., Dehaese, O., Tavernier, K., Macé, E., Even, J., Le Corre, A. and Loualiche, S., "Demonstration of a low threshold current in 1.54μm InAs/InP (311)B quantum dot laser with reduced number of stacks," Japanese J. of Appl. Phys. 46(10A), 6903-6905 (2007).

[3] Zhou, D., Piron, R., Grillot, F., Dehaese, O., Homeyer, E., Dontabactouny, M., Batte, T., Tavernier, K., Even, J. and Loualiche, S., "Study of the characteristics of 1.55μm quantum dash/dot semiconductor lasers on InP substrate," Appl. Phys. Lett. 93, 161104 (2008).

[4] Cornet, C., Schliwa, A., Even, J., Doré, F., Celebi, C., Létoublon, A., Macé, E., Paranthoen, C., Simon, A., Koenraad, P. M., Bertru, N., Bimberg, D. and Loualiche, S., "Electronic and optical properties of InAs/InP quantum dots on InP(100) and InP(113)B substrates : theory and experiment," Phys. Rev. B 74, 035312 (2006).

[5] Cornet, C., Schliwa, A., Hayne, M., Chauvin, N., Doré, F., Even, J., Moshchalkov, V. V., Bimberg, D., Bremond, G., Bru-Chevalier, C., Gendry, M. and Loualiche, S., "InAs/InP quantum dots : from single to coupled dots applications," Phys. Stat. Sol. (c) 3, 4039-4042 (2006).

[6] Miska, P., Even, J., Dehaese O. and Marie, X., "Carrier relaxation in InAs-InP quantum dots," Appl. Phys. Lett. 92, 191103 (2008).

[7] Miska, P., Even, J., Marie, X. and Dehaese O., "Electronic structure and carrier dynamics in InAs-InP double cap (113)B quantum dots," Appl. Phys. Lett. 94, 0611916 (2009).

[8] Ohnesorge, B., Albrecht, M., Oshinowo, J., Arakawa, Y. and Forchel, A., "Rapid carrier relaxation in self-assembled $In_xGa_{1-x}As$/GaAs quantum dots", Phys. Rev. B, 54(16) 11532-11538 (1996).

[9] Berg, T., Bischoff, S. , Magnusdottir, I. and Mork, "Ultrafast gain recovery and modulation limitations in self-assembled quantum-dot devices", J., IEEE Phot. Tech. Lett., 13(6), 541-543 (2001).

[10] Markus, A., Chen, J. X., Paranthoen, C., Fiore, A., Platz, C. and Gauthier-Lafaye, O., "Simultaneous two-state lasing in quantum-dot lasers", Appl. Phys. Lett., 82(12), 1818-1820 (2003).

[11] Platz, C., Paranthoen, C., Caroff, P., Bertru, N., Labbe, C., Even, J., Dehaese, O., Folliot, H., Le Corre, A., Loualiche, S., Moreau, G. , Simon, J. C. and Ramdane, A., Semicond. Sci. Technol., 20, 459-463 (2005).

[12] Veselinov, K., Grillot, F., Cornet, C., Even, J., Bekiarski, A., Gioannini, M. and Loualiche, S., "Analysis of the double laser emission occurring Fresnel in 1.55μm InAs-InP(113)B quantum dot lasers," IEEE Journal of Quantum Electronics 43(9), 810-816 (2007).

[13] Cornet, C., Labbé, C., Folliot, H., Bertru, N., Dehaese, O., Even, J., Le Corre, A., Paranthoen, C., Platz, C. and Loualiche, S., "Quantitative investigations of optical absorption in InAs/InP .311.B quantum dots emitting at 1.55 mm wavelength", Appl. Phys. Lett., 85(23), 5685-5687 (2004).

[14] Sugawara, M., Mukai, K., Nakata, Y. and Ishikawa, H., "Effect of homogeneous broadening of optical gain on lasing spectra in self assembled $In_xGa_{1-x}As$/GaAs quantum dot lasers ",Phys. Rev. B, 61(11) 7595-7603 (2000).

[15] Sugawara, M., Hatori, N. , Ebe, H. , Arakawa, Y. , Akiyama, T., Otsubo, K. and Nakata, K., "Modelling room-temperature lasing spectra of 1.3mm self assembled InAs/GaAs quantum dot lasers : homogeneous broadening of optical gain under current injection",Journal of Applied Physics, 97, 043523 (2005).

[16] Grillot, F., Veselinov, K., Gioannini, M, Montrosset, I, Even, J., Piron, R., Homeyer, E. and Loualiche, S., "Spectral analysis of 1.55μm InAs-InP(113)B quantum dot lasers based on a multipopulation rate equations model," IEEE Journal of Quantum Electronics 45(7), 872-878 (2009).

 [17] Cornet, C., Labbé, C., Folliot, H., Caroff, P., Levallois, C., Dehaese O., Even, J., Le Corre, A. and Loualiche, S., "Time-resolved pump probe of 1.55μm InAs/InP quantum dots under high resonant excitation," Appl. Phys. Lett. 88, 171502 (2008).

[18] Massé, N. F., Homeyer, E., Marko, I. P., Adams, A. R., Sweeney, S. J., Dehaese, O., Piron, R., Grillot, F. and Loualiche, S., "Temperature and pressure dependence of the recombination processes in 1.55μm InAs/InP (311)B quantum dot lasers," Appl. Phys. Lett. 91, 131113 (2006).

[19] Pan, J.L., "Intraband Auger processes and simple models of the ionization balance in semiconductor quantum-dot lasers", Phys. Rev. B49, 11272-11287 (1994)

[20] Even, J. Doré, F., Cornet, F. and Pédesseau, L., "Semianalytical model for simulation of electronic properties of narrow-gap strained semiconductor quantum nanostructures", Phys. Rev. B77, 085305 (2008)

[21] Grillot, F. Dagens, B., Provost, J. G., Su, H and Lester L. F., "Gain compression and above-threshold linewidth enhancement factor in 1.3μm InAs-GaAs quantum dot lasers", IEEE Journal of Quantum Electronics, 44(10), 946-951(2008).